

AD-A041 445

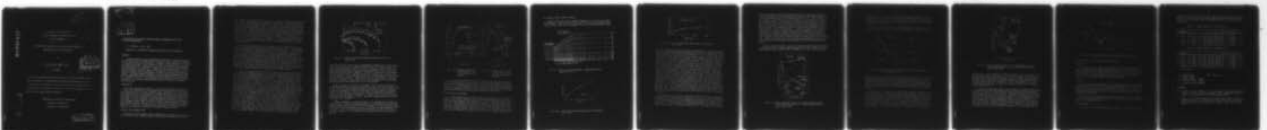
WASHINGTON UNIV SEATTLE DEPT OF MECHANICAL ENGINEERING F/G 20/11  
A PROCEDURE FOR EVALUATING FRACTURE DYNAMIC PARAMETERS FROM CRA--ETC(U)  
MAY 77 A S KOBAYASHI, S MALL N00014-76-C-0060

UNCLASSIFIED

TR-28

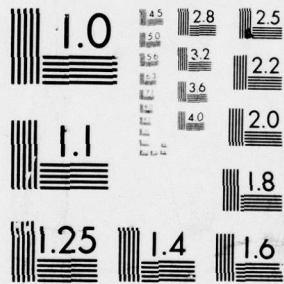
NL

| OF |  
AD  
A041445



END

DATE  
FILMED  
8 - 77



MICROCOPY RESOLUTION TEST CHART  
NATIONAL BUREAU OF STANDARDS-1963-A

ADA041445

15 Office of Naval Research

Contract N00014-76-C-0060 NR 064-478

9 Technical Report No. 28

14 TP-28

A PROCEDURE FOR EVALUATING FRACTURE DYNAMIC PARAMETERS  
FROM CRACK VELOCITY MEASUREMENTS

by

10 A.S. Kobayashi and S. Mall

11 May 1977

DDC  
RECEIVED  
JUL 11 1977  
RECEIVED

The research reported in this technical report was made possible through support extended to the Department of Mechanical Engineering, University of Washington, by the Office of Naval Research under Contract N00014-76-C-0060 NR 064-478. Reproduction in whole or in part is permitted for any purpose of the United States Government.

Department of Mechanical Engineering

College of Engineering

University of Washington

DISTRIBUTION STATEMENT A  
Approved for public release;  
Distribution Unlimited

SEARCHED		INDEXED	
SERIALIZED		FILED	
ADDITIONAL AVAILABILITY CODES			
1st. AVAIL. AND 2nd. SPECIAL			
A			

## A PROCEDURE FOR EVALUATING FRACTURE DYNAMIC PARAMETERS FROM CRACK VELOCITY MEASUREMENTS

A. S. Kobayashi and S. Mall

Department of Mechanical Engineering, University of Washington

### ABSTRACT

A combined numerical and experimental procedure for evaluating some of the fracture dynamic parameters which govern the crack run-arrest response in a fracturing plate are discussed. A dynamic finite element code is used to compute the dynamic stress intensity factor and dynamic energy release rate associated with a propagating crack which is driven by the experimentally determined crack velocity. Numerical results generated by the developed procedure are then compared with dynamic stress intensity factors obtained through dynamic photoelastic analyses of fracturing Homalite-100 plates. Two edge-cracked specimens with fixed edge displacement loadings and two wedge-loaded double cantilever beam specimens were considered in this comparative study. Good agreements were obtained between the results obtained by the developed numerical-experimental procedure and dynamic photoelasticity.

### INTRODUCTION

The three approaches currently in use in fracture dynamic studies are: to relate the experimentally determined crack velocities with static fracture parameters [1]; to relate experimentally determined crack velocities with those obtained from an analytical dynamic model without or with postulated dynamic fracture toughness [2,3,4]; and to determine experimentally the dynamic state of stress in fracturing polymeric materials [5,6,7]. In this paper, a fourth procedure, which utilizes the versatility of dynamic finite element method (FEM) to extract fracture dynamic parameters from the most commonly measured quantity of crack velocity in practical structural material is described. The procedure is then used to indicate the errors involved in using static analysis to interpret dynamic results.

### DYNAMIC FINITE ELEMENT CODE

The dynamic finite element method (FEM) which has evolved since its initial use [8] in this combined numerical-experimental procedure is the FEM

code HONDO [9] with artificial viscosity to reduce the keystone effect in the finite elements along the opening crack surfaces. In this dynamic FEM procedure, crack extension is modeled by discontinuous jumps of the crack tip from one finite element node to its adjacent node and the time-averaged crack tip displacement is equated to the average crack tip velocity at the adjacent node. The average work necessary to open the newly created increment of crack surface is then used to compute the surface energy dissipation rate which is equated to the dynamic energy release rate at the crack tip node just prior to the subsequent discrete movement of the crack tip [8]. An accuracy check of this direct procedure for computing the dynamic energy release rate was established by a comparative study with Baker's solution [10] where the numerical and theoretical results agreed within 1 percent of each other [8].

More recently another check on the dynamic finite element algorithm was made by comparing the crack opening displacements (COD) of a constant velocity crack against the theoretical solution of Broberg [11]. In this numerical study involving a fracturing steel plate, an artificial keystone viscosity of  $B3=0.2$  was used to damp out the keystone effect prevalent in previous analyses. The numerically determined time-averaged COD at every other node away from the moving crack tip was found to be in excellent agreement with Broberg's result for a crack velocity of  $c/c_1 = 0.076$  where  $c$  and  $c_1$  are the crack and dilatational wave velocities, respectively [12]. It was also shown that at this low crack velocity, the stress intensity factor computed by static near field solution was only 2.2 percent higher than that computed by the dynamic near field solution when dynamic finite element COD values were used to compute the dynamic stress intensity factor.

In order to examine further the effectiveness of the above COD technique in dynamic finite element analysis of fracturing Homalite-100 plates, the well analyzed fracturing dynamic photoelastic specimens B2 and B13 [8] were reanalyzed with various artificial viscosities. The finite element breakdown and the crack velocities used in this new study are identical to those used in Reference [8]. Figure 1 shows the crack opening displacements at three crack lengths in Specimen B2 with three artificial viscosities. The small artificial viscosity of  $B3 = 0.01$  and  $0.1$  were not very effective in removing keystone but the prominent fluctuations in COD were substantially suppressed with  $B3 = 0.5$ . It should also be noted that a significant change was made in the numerical algorithm where the initial residual surface tractions along crack propagation were computed by using a static modulus of elasticity of  $E_s = 540$  ksi while all stress wave propagation induced by the running crack were computed with a dynamic modulus of elasticity of  $E_p = 675$  ksi. This combined use of static and dynamic moduli of elasticity in dynamic finite element analysis, initially proposed by Gehlen [13], is an attempt to model the strain rate sensitivity of the modulus of elasticity of Homalite-100 material. Such strain rate sensitivity did not exist in the fracture dynamic analysis of steel tapered DCB specimen [12] which is easier to analyze by dynamic finite element analysis than the photoelastic specimens. Our continuing interest in using dynamic photoelasticity to study fracture dynamics despite the added complexity of strain rate sensitivity

Unclassified

SECURITY CLASSIFICATION OF THIS PAGE (When Data Entered)

REPORT DOCUMENTATION PAGE

1. REPORT NUMBER

2. GOVT ACCESSION NO.

READ INSTRUCTIONS  
BEFORE COMPLETING FORM  
3. RECIPIENT'S CATALOG NUMBER

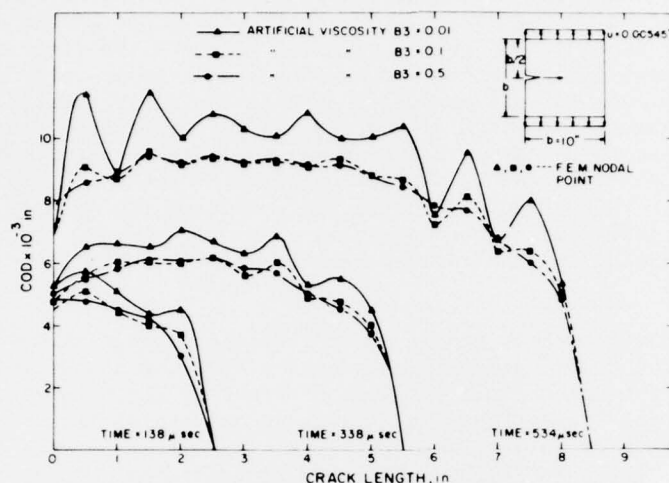


Fig. (1) - Effect of artificial keystone viscosity on COD in Test No. B2.

stems from the fact that no other experimental technique can provide an accurate near field state of stress in the vicinity of a running crack. Dynamic photoelasticity is one of few optical techniques which can provide experimentally determined dynamic stress intensity factor with which our numerical results could be compared. As will be shown later, such dynamic stress intensity factors computed through the combined use of static and dynamic moduli of elasticity agreed well with the experimental results under the state of plane strain. The latter state of plane strain for thicker Homalite-100 plates is considered to be a better modeling of the cleavage fractured surface observed in the fractured specimens.

Figure 2 shows the variations in dynamic stress intensity factors obtained numerically by the energy release rate method [8] and COD method [12] as well as their experimental counterpart determined by dynamic photoelasticity for Specimen B2. While the two numerical algorithms of computing dynamic stress intensity factors do not yield substantially different results, the more pronounced fluctuation in dynamic stress intensity factors computed by the COD method is noted. Thus this comparison favors the energy release rate procedure.

Likewise comparison is shown in Figure 3 for Specimen B13 in which the crack arrested. While the prominent peak in the experimentally determined dynamic stress intensity factor was not observed in the two numerical values, the experimental and numerical results are otherwise in good agreement with each other. Again the numerical results obtained by energy release rate procedure appears to be in slightly better agreement with the experimental results.

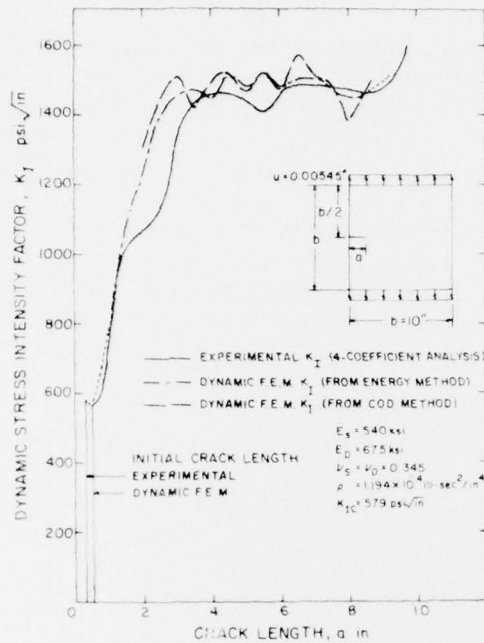


Fig. (2) - Dynamic stress intensity factors in Test No. B2, plane strain analysis

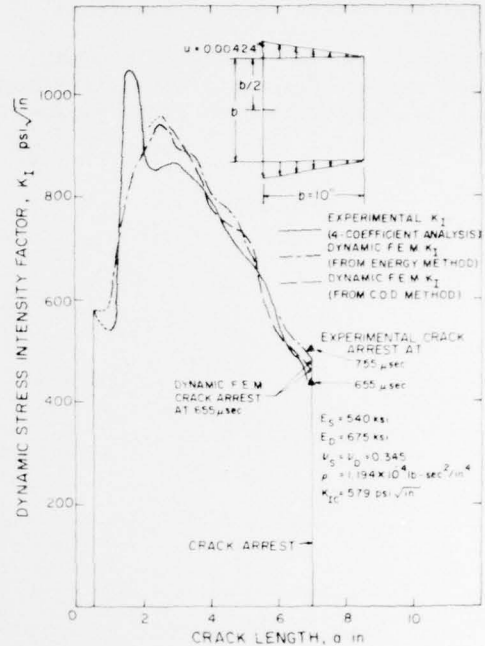


Fig. (3) - Dynamic stress intensity factors in Test No. B13, plane strain analysis

As a result of these two comparative studies using the well analyzed specimens B2 and B13, it was concluded that the energy release rate procedure provided slightly better numerical results of the fracturing Homalite-100 plates. This conclusion unfortunately differs with that in Reference [12] and is perhaps indicative of the larger keystone effect in the Homalite-100 plates due to its much smaller modulus of elasticity.

#### WEDGE-LOADED DCB SPECIMEN

The above dynamic finite element algorithm was then used to analyze the dynamic crack arrest results of two wedge-loaded double cantilever beam (DCB) specimens machined from Homalite-100 plates of 1/2 inch nominal thickness [14]. The dynamic stress intensity factors of these two fracturing tapered DCB specimens were determined by a different data reduction scheme of dynamic photoelasticity results than that used by the authors [7]. The static and dynamic material properties as well as the crack position versus time relations reported in Reference [14] were used as input conditions to

our dynamic finite element analysis.

Figure 4 shows the finite element breakdown of one of the two tapered DCB specimens. Figures 5(a) and (b) show the crack position versus time relations which were used to propagate the crack tip intermittently along

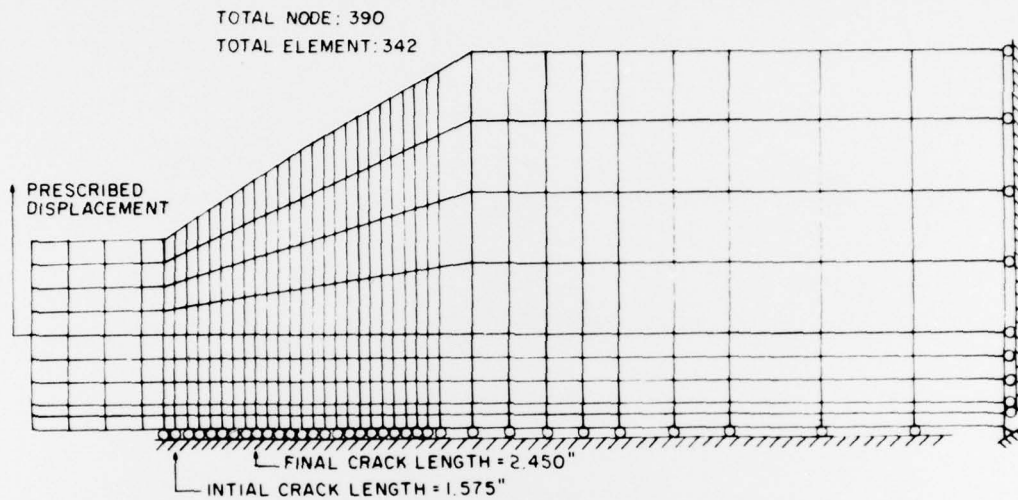


Fig. (4) - Finite element breakdown of wedge-loaded C-DCB model No. 7 [14]

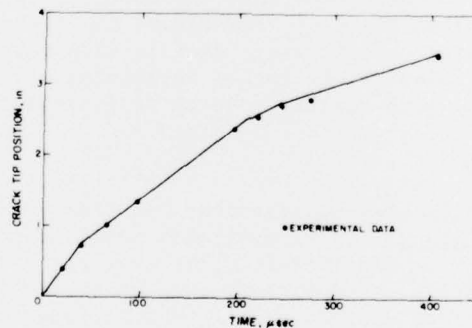


Fig. 5(a) - Crack tip position versus time in C-DCB model No. 6 [14]

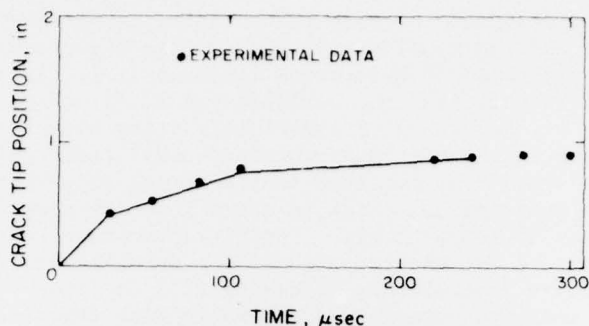


Fig. 5(b) - Crack tip position versus time in C-DCB model No. 7 [14]

the finite element nodes at prescribed time intervals. Fixed pin displacements were prescribed during the entire fracture process which were 459 and 300 microseconds for Specimens C-DCB Model Nos. 6 and 7, respectively. This assumption of fixed grip condition has been the source of discussion since one of the authors presented a dynamic finite element analysis of the crack propagation and arrest in a tapered DCB specimen using measured crack velocities [15]. The static stress intensity factor at crack arrest computed under the assumption of fixed grip condition was approximately 40 percent lower than the corresponding value computed under the assumption of variable load condition of Reference [16], thus indicating the sensitivity of the arrest stress intensity factor to the prescribed boundary condition during crack propagation in such small crack arrest specimen. Subsequent analysis of another tapered DCB specimen under the two different loading conditions of our fixed grip loading and the variable loading condition prescribed in References [16] and [17] showed that while the dynamic strains computed under the former condition agreed well with the three strain gage measurements [16], the corresponding dynamic strains computed under the assumption of variable loading differed considerably with experimental results [12]. As a result of this analysis [12], the fixed grip condition is believed to be a valid assumption in the series of experiments reported in Reference [16]. This conclusion also indicates that the crack arrest stress intensity factor determined by the procedure described in References [16] and [17] could grossly overestimate the crack arrest potential of the material tested.

Unfortunately, the excellent agreements between the crack arrest stress intensity factors determined by simulations of the crack arrest experiments of References [16] and [17] using Homalite-100 specimens [14] and the crack arrest stress intensity factors determined independently by dynamic photoelasticity [5] have been used as experimental evidence for justifying the variable pin loading in References [16] and [17]. A cursory study, however,

shows considerable differences between the relative compliances between the loading fixture and the Homalite-100 specimen in the dynamic photoelasticity experiments and those of References [16] and [17]. As a result, one can conclude qualitatively that the variable pin loads measured in the rigid loading fixture of the simulated experiments using Homalite-100 specimens should be closer to the pin loads obtained under fixed grip condition while such condition cannot be realized in the actual experiments using steel specimen. An experimental check in these relative compliances can be easily made to verify such hypothesis. Another procedure is to analyze numerically the fracture dynamic response of the Homalite-100 specimens following the procedure described in Reference [15] and then identify the differences or similarities between these results with those of Reference [12]. Dynamic finite element analyses under the fixed grip condition should thus provide this insight into the controversy surrounding the exact boundary conditions on the tapered DCB specimens used in crack arrest experiments.

Figure 6 shows the dynamic and static stress intensity factors obtained by static and dynamic finite element analyses under the assumption of fixed grip condition for a Homalite-100 C-DCB Model No. 6 [14]. Also shown are

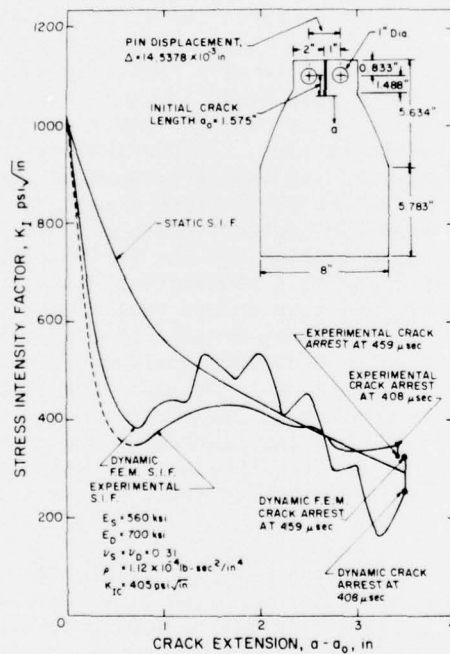


Fig. (6) - Stress intensity factors in a wedge-loaded contoured DCB specimen (Model No. 6). Load at fracture initiation = 151 lb [14].

the dynamic stress intensity factors of this specimen obtained by dynamic photoelasticity [14]. While the numerically obtained dynamic stress intensity factors show some small oscillations, the two results are generally in qualitative agreement with each other and in particular are in excellent agreement at crack arrest.

Figure 7 shows the crack opening displacements (COD) of the same specimen. As expected, the keystoneing effect continues to increase with

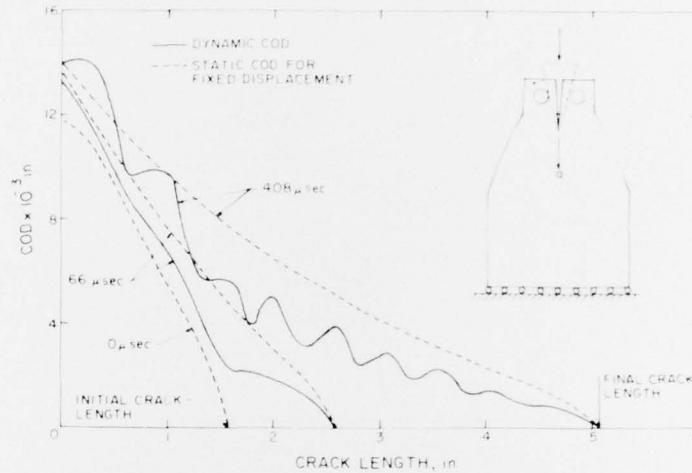


Fig. (7) - Crack opening displacement (COD) at different times in C-DCB Model No. 6 [14]

increase in crack length despite the high artificial viscosity of  $B3 = 0.5$ . The pronounced smaller dynamic crack opening displacements, which was also observed in the metallic specimens [12,15], in this cantilever beam type specimen are indications of the delayed response of the propagating crack tip to the applied load at the loading pin. Such delay response further verifies our assumed fixed grip loading condition during crack propagation and arrest.

Figure 8 shows the dynamic and static stress intensity factors in Specimen C-DCB Model No. 7. Again, relatively good agreement, particularly at crack arrest, between the experimental and numerical results is noted. The rapid small oscillations in dynamic stress intensity factors, which were noted in Figure 6, are absent in Figure 8. Our past experiences in numerical fracture dynamic analyses [4, 12] indicate that smoothed crack velocities generally result in oscillations in dynamic stress intensity factors and vice versa. Since the test results of Model C-DCB No. 6 recorded 9 crack positions for a crack extension of 3.41 in. while 7 crack positions are

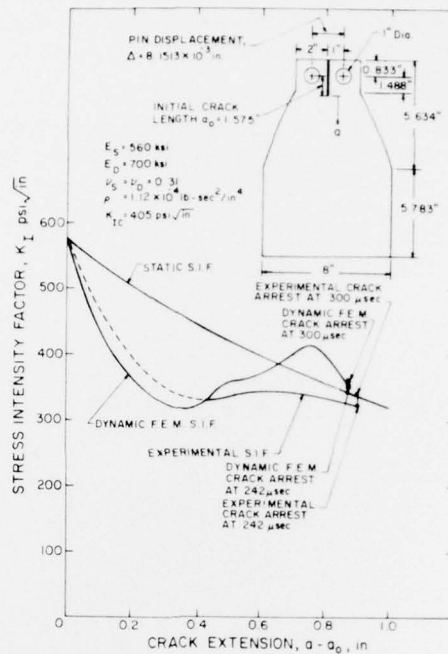


Fig. (8) - Stress intensity factors in a wedge-loaded contoured DCB specimen (Model No. 7). Load at fracture initiation = 89 lb [14].

recorded for a crack extension of 0.90 in. for Model 7, one would expect the crack position versus time relation for the test of Model 6 to represent a smoother time average position instead of a more precise crack position versus time relation necessary to generate a smoothly varying dynamic stress intensity as was the case of Model No. 7 test. Thus Model No. 7 should yield smoother variations in numerically computed dynamic stress intensity factor than Model No. 6.

The above good agreement between the variations in dynamic stress intensity factors with crack propagation obtained numerically and experimentally verifies the validity of the fixed grip condition under which the dynamic stress intensity factors were computed. Although the numerical results provide the variations in pin loads with respect to crack propagation as shown in Figure 9, corresponding experimental results were not available for direct comparison. Thus experimentally measured pin load from a separate test [14] is shown in Figure 9 for qualitative comparison. The two-fold differences between ringing frequencies of the numerical and experimental pin loads could be due to unavoidable compliance of the loading frame and

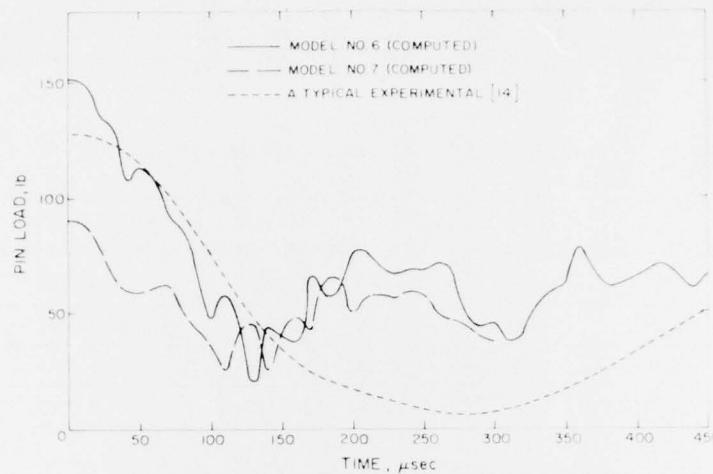


Fig. (9) - Pin load versus time in wedge-loaded C-DCB specimens

load cell system in the actual experimental setup.

#### DISCUSSION

An internal accuracy check of the dynamic finite element algorithm was made by computing the instantaneous energy balance of the entire system. Typical results for four crack lengths are shown in Tables 1 and 2. It is interesting to note that the accuracy of this energy balance is somewhat lower for Model No. 6 specimen which also showed larger oscillation in dynamic stress intensity factors with crack propagation.

#### CONCLUSIONS

A dynamic finite element algorithm has been developed for computing the dynamic stress intensity factors from experimentally determined crack position versus the relation of a propagating and arresting crack. Accuracy of the developed numerical procedure was checked by comparing the numerically determined stress intensity factors with those determined in four dynamic photoelastic experiments.

The numerically and experimentally determined dynamic stress intensity factors of two wedge-loaded DCB specimens indicate that the crack propagates under a fixed grip condition.

#### ACKNOWLEDGEMENT

The results of this investigation were obtained in a research contract

funded by the Office of Naval Research under Contract No. N00014-76-C-0060, NR 064-478. The authors wish to acknowledge the support and encouragement of Drs. N.R. Perrone and D. Mulville of ONR during the course of this investigation.

TABLE 1 - ENERGY BALANCE IN C-DCB MODEL NO. 6

Crack Extension	W	U	K	F	$(U + K + F)/W - 1$
1.0	3.201	2.221	0.223	0.534	- 0.070
2.0	3.201	1.956	0.074	0.879	- 0.091
3.0	3.201	1.748	0.038	1.114	- 0.094
3.5*	3.201	1.629	0.055	1.154	- 0.113

TABLE 2 - ENERGY BALANCE IN C-DCB MODEL NO. 7

Crack Extension	W	U	K	F	$(U + K + F)/W - 1$
0.25	1.084	0.957	0.015	0.079	- 0.033
0.50	1.084	0.867	0.034	0.116	- 0.067
0.75	1.084	0.855	0.015	0.155	- 0.059
0.875*	1.084	0.836	0.005	0.181	- 0.062

### \* Crack Arrest

W: External Work                      Unit: Pound-in.  
U: Strain Energy  
K: Kinetic Energy  
F: Fracture Energy  $\equiv \int_0^c$   
c: Length of Crack Extension

## REFERENCES

- [1] Crosley, P.B. and Ripling, E.J., "Plane strain crack arrest characterizations of steels", Journal of Pressure Vessel Technology, Trans. of ASME, Vol. 97, Series J, pp. 291-298, November 1975.
- [2] Burns, S.J., "Crack propagation in rapidly wedged double cantilevered beam specimens", Proc. of 12th Annual Meeting of the Society of Engineering Sciences, The University of Texas at Austin, pp. 121-129, 1975.

- [3] Hoagland, R.G., Gehlen, R.C., Rosenfield, A.R. and Hahn, G.T., "The application of D.C.B. specimens for measuring the crack arrest properties of A533B and other steels", to be published in Fast Fracture and Crack Arrest, ASTM STP 627, 1977.
- [4] Emery, A.F., Love, W.J. and Kobayashi, A.S., "Influence of dynamic fracture toughness on elastic crack propagation in a pressurized crack", to be published in the Proc. of the International Conference on Fracture Mechanics and Technology, Hong Kong, March 21-25, 1977.
- [5] Kobayashi, T. and Dally, J.W., "The relation between crack velocity and stress intensity factor in birefringent polymers", to be published in Fast Fracture and Crack Arrest, ASTM STP 627, 1977.
- [6] Kalthoff, J.F., Beinert, J. and Winkler, S., "Dynamic stress intensity factors for arresting cracks in DCB specimens", *ibid loc cit*.
- [7] Kobayashi, A.S. and Mall, S., "Dynamic stress intensity factor of Homalite-100", presented at 1977 SESA Spring Meeting, May 16-20, 1977, Dallas, Texas.
- [8] Kobayashi, A.S., Emery, A.F. and Mall, S., "Dynamic finite element and dynamic photoelastic analyses of two fracturing Homalite-100 plates", *Experimental Mechanics*, Vol. 16, No. 9, pp. 321-328, September 1976.
- [9] Keys, S.W., "HONDO - A finite element computer program for large deformation dynamic response of axisymmetric solids", Sandia Laboratories Rep. SLA-74-0039, April 1974.
- [10] Baker, B.R., "Dynamic stresses created by a moving crack", *J. of Applied Mechanics*, Trans. of ASME, Vol. 29, Series E, pp. 449-458, September 1962.
- [11] Broberg, K.B., "The propagation of a brittle crack", *Arkiv-fur-Fysik*, Vol. 18, pp. 159-198, 1960.
- [12] Urabe, Y., Kobayashi, A.S., Emery, A.F. and Love, W.J., "Further dynamic finite element analysis of the tapered DCB specimen", submitted for publication in *Trans. of ASME*.
- [13] Hahn, G.T., Gehlen, P.C., Hoagland, R.G., Marschall, C.W., Kanninen, M.F., Popelar, C. and Rosenfield, A.R., "Critical experiments and analyses to establish a crack arrest methodology for nuclear pressure vessel steels", BMI-NUREG-1959, Battelle Columbus Laboratories Report, pp. 2-45-2-71, October 1976.
- [14] Irwin, G.R., Dally, J.W., Kobayashi, T., Fournery, W.L. and Etheridge, J.M., "A photoelastic characterization of dynamic fracture", NUREG-0072, U.S. Nuclear Regulatory Commission, December 1976.

- [15] Urabe, Y., Kobayashi, A.S., Emery, A.F. and Love, W.J., "Dynamic finite element analysis of a tapered DCB specimen", to be published in the Proc. of the International Conference on Fracture Mechanics and Technology, Hong Kong, March 21-25, 1977.
- [16] Crosley, P.B. and Ripling, E.J., "Characteristics of a run-arrest segment of crack extension", to be published in Fast Fracture and Crack Arrest, ASTM STP 627, 1977.
- [17] Crosley, P.B. and Ripling, E.J., "Towards development of a standard test for measuring  $K_{Ia}$ ", *ibid loc cit.*

#### Administrative & Liaison Activities

Chief of Naval Research  
Department of the Navy  
Arlington, Virginia 22217  
Attn: Code 474 (2)  
471  
212

Director  
ONR Branch Office  
445 Summer Street  
Boston, Massachusetts 02210

Director  
Naval Research Laboratory  
Attn: Code 2629 (ONRL)  
Washington, D.C. 20390 (6)

U.S. Naval Research Laboratory  
Attn: Code 2627  
Washington, D.C. 20390

Director  
ONR - New York Area Office  
713 Broadway - 5th Floor  
New York, N.Y. 10003

Director  
ONR Branch Office  
1300 E. Green Street  
Pasadena, California 91101

Defense Documentation Center  
Cameron Station  
Alexandria, Virginia 22304 (12)

#### ASST

Commanding Officer  
U.S. Army Research Office Durham  
Attn: Mr. J.L. Murray  
CRD-AR-12  
Box CM, Duke Station  
Durham, North Carolina 27706 (2)

Commanding Officer  
ADCON-621  
Attn: Mr. R. Shea  
US Army Materials Res. Agency  
Watertown, Massachusetts 02172

#### Air Force

Command WADD  
Wright-Patterson Air Force Base  
Dayton, Ohio 45433  
Attn: Code 450000

AFPHL (FDDH)  
Structures Division  
APLC (MCEEA)

Chief, Applied Mechanics Group  
U.S. Air Force Inst. of Tech.  
Wright-Patterson Air Force Base  
Dayton, Ohio 45433

Chief, Civil Engineering Branch  
WAC, Research Division  
Air Force Weapons Laboratory  
Griest AFB, New Mexico 87117

Air Force Office of Scientific Research  
1000 Wilson Blvd.  
Arlington, Virginia 22209  
Attn: Mechanics Div.

#### ASST

Structures Research Division  
National Aeronautics & Space Admin.  
Langley Research Center  
Langley Station  
Hampton, Virginia 23065

National Aeronautics & Space Admin.  
Research Administrator for Advanced  
Research & Technology  
Washington, D.C. 20546

Scientific & Tech. Info. Facility  
NASA Representative (S-AK/DL)  
P.O. Box 1700  
Bethesda, Maryland 20014

#### Other Government Activities

Commandant  
Chief, Testing & Development Div.  
U.S. Coast Guard  
1300 E. Street, N.W.  
Washington, D.C. 20226

Technical Director  
Marine Corps Dev. & Educ. Command  
Quantico, Virginia 22134

#### Watervliet Arsenal

MA&S Research Center  
Watervliet, New York 12189  
Attn: Director of Research

#### Technical Library

Bedstone Scientific Info. Center  
Chief, Document Section  
U.S. Army Missile Command  
Redstone, Arsenal, Alabama 35809

Army R&D Center  
Fort Belvoir, Virginia 22060

#### Navy

Commanding Officer and Director  
Naval Ship Research & Development Center  
Bethesda, Maryland 20034  
Attn: Code 042 (Tech. Lib. Br.)

17  
172  
174  
177  
1800 (Appl. Matn. Lab.)  
54125 (Dr. W.D. Sette)  
19  
1901 (Dr. M. Strassberg)  
1945  
196  
1962

Naval Weapons Laboratory  
 Dahlgren, Virginia 22448

Naval Research Laboratory  
Washington, D.C. 20375  
Attn: Code 8400

8410  
8410  
8440  
6300  
6390  
6380

#### Undersea Explosion Research Div.

Naval Ship R&D Center  
Norfolk Naval Shipyard  
Portsmouth, Virginia 23709  
Attn: Dr. E. Palmer  
Code 780

#### Naval Ship Research & Development Center

Annapolis Division  
Annapolis, Maryland 21402  
Attn: Code 2740 - Dr. Y.F. Wang  
28 - Mr. R.J. Wolfe  
281 - Mr. R.B. Niederberger  
2814 - Dr. R. Vanderveldt

#### Technical Library

Naval Underwater Weapons Center  
Pasadena Annex  
3202 E. Foothill Blvd.  
Pasadena, California 91107

U.S. Naval Weapons Center  
China Lake, California 93557  
Attn: Code 4062 - Mr. W. Werback  
4520 - Mr. Ken Bischof

Commanding Officer  
U.S. Naval Civil Engr. Lab  
Code L31  
Port Hueneme, California 93041

Technical Director  
U.S. Naval Ordnance Laboratory  
White Oak  
Silver Spring, Maryland 20910

Technical Director  
Naval Undersea R&D Center  
San Diego, California 92132

Supervisor of Shipbuilding  
U.S. Navy  
Newport News, Virginia 23607

Technical Director  
Mare Island Naval Shipyard  
Vallejo, California 94592

U.S. Navy Underwater Sound Ref. Lab.  
Office of Naval Research  
PO Box 8337  
Orlando, Florida 32806

Chief of Naval Operations  
Dept. of the Navy  
Washington, D.C. 20350  
Attn: Code Op071

Strategic Systems Project Office  
Department of the Navy  
Washington, D.C. 20360  
Attn: NSP-001 Chief Scientist

#### Deep Submergence Systems

Naval Ship Systems Command  
Code 39522  
Department of the Navy  
Washington, D.C. 20360

Engineering Dept.  
US Naval Academy  
Annapolis, Maryland 21402

Naval Air Systems Command  
Dept. of the Navy  
Washington, D.C. 20360

Attn: NAVAIR 5302 Aero & Structures  
5308 Structures  
520317 Materials  
604 Tech. Library  
3208 Structures

Director, Aero Mechanics  
Naval Air Development Center  
Johnsville  
Harrisburg, Pennsylvania 17174

Technical Director  
U.S. Naval Undersea R&D Center  
San Diego, California 92132

Engineering Department  
U.S. Naval Academy  
Annapolis, Maryland 21402

Naval Facilities Engineering Command  
Dept. of the Navy  
Washington, D.C. 20360

Attn: NAVFAC 9, Research & Development  
94  
14414 Tech. Library

#### Naval Sea Systems Command

Dept. of the Navy  
Washington, D.C. 20360

Attn: NAVSHIP 03 Res. & Technology  
011 Ch. Scientist for R&D  
03412 Hydromechanics  
037 Ship Silencing Div.  
035 Weapons Dynamics

Naval Ship Engineering Center  
Prince Georges' Plaza  
Hyattsville, Maryland 20782

Attn: NAVSEC 6100 Ship Sys. Engr. & Des. Div.  
6102C Computer-Aided Ship Des.  
6105C  
6110 Ship Concept Design  
6120 Hull Div.  
6120B Hull Div.  
6126 Surface Ship Struct.  
6129 Submarine Struct.

PART 2 - CONTRACTORS AND OTHER  
TECHNICAL COLLABORATORS

Universities

Dr. J. Tinsley Olsen  
University of Texas at Austin  
343 Eng. Science Bldg.  
Austin, Texas 78712

Prof. Julius Miklowitz  
California Institute of Technology  
Div. of Engineering & Applied Sciences  
Pasadena, California 91109

Dr. Harold Liebowitz, Dean  
School of Engr. & Applied Science  
George Washington University  
725 23rd St. N.W.  
Washington, D.C. 20006

Prof. Eli Sternberg  
California Institute of Technology  
Div. of Engr. & Applied Sciences  
Pasadena, California 91109

Prof. Paul M. Naghi  
University of California  
Div. of Applied Mechanics  
Kitcher Hall  
Berkeley, California 94720

Professor P.S. Symonds  
Brown University  
Division of Engineering  
Providence, R.I. 02912

Prof. A.J. Durelli  
The Catholic University of America  
Civil/Mechanical Engineering  
Washington, D.C. 20017

Prof. R.B. Testa  
Columbia University  
Dept. of Civil Engineering  
S.W. Mudd Bldg.  
New York, N.Y. 10027

Prof. H.H. Bleich  
Columbia University  
Dept. of Civil Engineering  
Amsterdam & 120th St.  
New York, N.Y. 10027

Librarian  
Webb Institute of Naval Architecture  
Crescent Beach Road, Glen Cove  
Long Island, New York 11542

Prof. Daniel Frederick  
Virginia Polytechnic Institute  
Dept. of Engineering Mechanics  
Blacksburg, Virginia 24061

Prof. A.C. Eringen  
Dept. of Aerospace & Mech. Sciences  
Princeton University  
Princeton, New Jersey 08540

Dr. S.L. Koh  
School of Aero., Astro. & Engr. Sci.  
Purdue University  
Lafayette, Indiana

Prof. E.H. Lee  
Div. of Engr. Mechanics  
Stanford University  
Stanford, California 94305

Prof. R.D. Mindlin  
Dept. of Civil Engineering  
Columbia University  
S.W. Mudd Building  
New York, N.Y. 10027

Prof. S.B. Dong  
University of California  
Dept. of Mechanics  
Los Angeles, California 90024

Prof. Burt Paul  
University of Pennsylvania  
Towne School of Civil & Mech. Engr.  
Rm. 113 - Towne Building  
220 S. 33rd Street  
Philadelphia, Pennsylvania 19104

Prof. H.W. Liu  
Dept. of Chemical Engineering & Metall.  
Syracuse University  
Syracuse, N.Y. 13210

Prof. S. Bodner  
Technion R&D Foundation  
Haifa, Israel

Prof. R.J.H. Bolland  
Chairman, Aeronautical Engr. Dept.  
207 Guggenheim Hall  
University of Washington  
Seattle, Washington 98195

Prof. F.L. DiMaggio  
Columbia University  
Dept. of Civil Engineering  
616 Mudd Building  
New York, N.Y. 10027

Prof. A.M. Freudenthal  
George Washington University  
School of Engineering & Applied Science  
Washington, D.C. 20006

D.C. Evans  
University of Utah  
Computer Science Division  
Salt Lake City, Utah 84112

Prof. Norman Jones  
Massachusetts Inst. of Technology  
Dept. of Naval Architecture & Marine Engineering  
Cambridge, Massachusetts 02139

Professor Albert I. King  
Biomechanics Research Center  
Wayne State University  
Detroit, Michigan 48202

Dr. V.R. Hodgson  
Wayne State University  
School of Medicine  
Detroit, Michigan 48202

Dean S.A. Boley  
Northwestern University  
Technological Institute  
2145 Sheridan Road  
Evanston, Illinois 60201

Prof. P.G. Hodge, Jr.  
University of Minnesota  
Dept. of Aerospace Engr. & Mechanics  
Minneapolis, Minnesota 55455

Dr. D.C. Drucker  
University of Illinois  
Dean of Engineering  
Urbana, Illinois 61801

Prof. N.M. Newmark  
University of Illinois  
Dept. of Civil Engineering  
Urbana, Illinois 61801

Prof. E. Reissner  
University of California, San Diego  
Dept. of Applied Mechanics  
La Jolla, California 92037

Prof. G.S. Heller  
Division of Engineering  
Brown University  
Providence, Rhode Island 02912

Prof. Werner Goldsmith  
Dept. of Mechanical Engineering  
Div. of Applied Mechanics  
University of California  
Berkeley, California 94720

Prof. J.R. Rice  
Division of Engineering  
Brown University  
Providence, Rhode Island 02912

Prof. R.S. Rivlin  
Center for the Application of Mathematics  
Lehigh University  
Bethlehem, Pennsylvania 18015

Library (Code 0384)  
U.S. Naval Postgraduate School  
Monterey, California 93940

Dr. Francis Cozzarelli  
Div. of Interdisciplinary Studies & Research  
School of Engineering  
State University of New York  
Buffalo, N.Y. 14214

Industry and Research Institutes

Library Services Department  
Report Section Bldg. 14-14  
Argonne National Laboratory  
9700 S. Cass Avenue  
Argonne, Illinois 60440

Dr. M.C. Junger  
Cambridge Acoustical Associates  
129 Mount Auburn St.  
Cambridge, Massachusetts 02138

Dr. L.H. Chen  
General Dynamics Corporation  
Electric Boat Division  
Groton, Connecticut 06340

Dr. J.E. Greenspan  
J.G. Engineering Research Associates  
3831 Menlo Drive  
Baltimore, Maryland 21215

Dr. S. Baldorf  
The Aerospace Corp.  
P.O. Box 92957  
Los Angeles, California 90009

Prof. William A. Nash  
University of Massachusetts  
Dept. of Mechanics & Aerospace Engr.  
Amherst, Massachusetts 01002

Library (Code 0384)  
U.S. Naval Postgraduate School  
Monterey, California 93940

Prof. Arnold Allentuch  
Newark College of Engineering  
Dept. of Mechanical Engineering  
123 High Street  
Newark, New Jersey 07102

Dr. George Herrmann  
Stanford University  
Dept. of Applied Mechanics  
Stanford, California 94305

Prof. J.D. Achenbach  
Northwestern University  
Dept. of Civil Engineering  
Evanston, Illinois 60201

Director, Applied Research Lab.  
Pennsylvania State University  
P.O. Box 30  
State College, Pennsylvania 16801

Prof. Eugen J. Skudrzyk  
Pennsylvania State University  
Applied Research Laboratory  
Dept. of Physics - P.O. Box 30  
State College, Pennsylvania 16801

Prof. J. Kempner  
Polytechnic Institute of Brooklyn  
Dept. of Aero. Engr. & Applied Mech.  
333 Jay Street  
Brooklyn, N.Y. 11201

Prof. J. Klossner  
Polytechnic Institute of Brooklyn  
Dept. of Aerospace & Appl. Mech.  
333 Jay Street  
Brooklyn, N.Y. 11201

Prof. R.A. Schapery  
Texas A&M University  
Dept. of Civil Engineering  
College Station, Texas 77840

Prof. W.D. Pilkey  
University of Virginia  
Dept. of Aerospace Engineering  
Charlottesville, Virginia 22903

Dr. H.G. Schaeffer  
University of Maryland  
Aerospace Engineering Dept.  
College Park, Maryland 20742

Prof. K.D. Willmert  
Clarkson College of Technology  
Dept. of Mechanical Engineering  
Putnam, N.Y. 13676

Dr. J.A. Stricklin  
Texas A&M University  
Aerospace Engineering Dept.  
College Station, Texas 77843

Dr. L.A. Schmit  
University of California, LA  
School of Engineering & Applied Science  
Los Angeles, California 90024

Dr. H.A. Kamel  
The University of Arizona  
Aerospace & Mech. Engineering Dept.  
Tucson, Arizona 85721

Dr. B.S. Berger  
University of Maryland  
Dept. of Mechanical Engineering  
College Park, Maryland 20742

Prof. G.R. Irwin  
Dept. of Mechanical Engineering  
University of Maryland  
College Park, Maryland 20742

Dr. S.J. Fenves  
Carnegie-Mellon University  
Dept. of Civil Engineering  
Schenley Park  
Pittsburgh, Pennsylvania 15213

Dr. Ronald L. Huston  
Dept. of Engineering Analysis  
Mail Box 112  
University of Cincinnati  
Cincinnati, Ohio 45221

Prof. George Sih  
Dept. of Mechanics  
Lehigh University  
Bethlehem, Pennsylvania 18015

Prof. A.S. Kobayashi  
University of Washington  
Dept. of Mechanical Engineering  
Seattle, Washington 98195

Mr. P.C. Durup  
Lockheed-California Company  
Aeromechanics Dept., 14-43  
Burbank, California 91503

Addendum:  
Assistant Chief for Technology  
Office of Naval Research, Code 280  
Arlington, Virginia 22217

Dr. K.C. Park  
Lockheed Palo Alto Research Laboratory  
Dept. 5233, Bldg. 205  
3251 Hanover Street  
Palo Alto, California 94304

Library  
Newport News Shipbuilding and Dry Dock Co.  
Newport News, Virginia 23607

Dr. W.F. Bozich  
McDonnell Douglas Corporation  
5301 Soledad Ave.  
Huntington Beach, California 92647

Dr. H.N. Abramson  
Southwest Research Institute  
Technical Vice President  
Mechanical Sciences  
P.O. Drawer 28510  
San Antonio, Texas 78284

Dr. R.C. DeHart  
Southwest Research Institute  
Dept. of Structural Research  
PO Drawer 28510  
San Antonio, Texas 78284

Dr. M.L. Baron  
Weidinger Associates,  
Consulting Engineers  
110 East 59th Street  
New York, N.Y. 10022

Dr. W.A. von Riesenmann  
Sandia Laboratories  
Sandia Base  
Albuquerque, New Mexico 87115

Dr. T.L. Geers  
Lockheed Missiles & Space Co.  
Palo Alto Research Laboratory  
3251 Hanover Street  
Palo Alto, California 94304

Dr. J.L. Tocher  
Boeing Computer Services, Inc.  
P.O. Box 24346  
Seattle, Washington 98124

Mr. William Caywood  
Code HBE, Applied Physics Laboratory  
8621 Georgia Avenue  
Silver Spring, Maryland 20904

Unclassified

SECURITY CLASSIFICATION OF THIS PAGE (When Data Entered)

REPORT DOCUMENTATION PAGE		READ INSTRUCTIONS BEFORE COMPLETING FORM
1. REPORT NUMBER TR No. 28	2. GOVT ACCESSION NO.	3. RECIPIENT'S CATALOG NUMBER TR-28
4. TITLE (and Subtitle) A Procedure for Evaluating Fracture Dynamic Parameters from Crack Velocity Measurements		5. TYPE OF REPORT & PERIOD COVERED Interim Report
		6. PERFORMING ORG. REPORT NUMBER
7. AUTHOR(s) A.S. Kobayashi and S. Mall		8. CONTRACT OR GRANT NUMBER(s) N00014-76-C-0060 NR 064-478
9. PERFORMING ORGANIZATION NAME AND ADDRESS University of Washington Department of Mechanical Engineering Seattle, Washington 98195		10. PROGRAM ELEMENT, PROJECT, TASK AREA & WORK UNIT NUMBERS
11. CONTROLLING OFFICE NAME AND ADDRESS Office of Naval Research Arlington, Virginia		12. REPORT DATE May 1977
		13. NUMBER OF PAGES 13
14. MONITORING AGENCY NAME & ADDRESS (if different from Controlling Office)		15. SECURITY CLASS. (of this report)
		15a. DECLASSIFICATION/DOWNGRADING SCHEDULE
16. DISTRIBUTION STATEMENT (of this Report)  Unlimited		
17. DISTRIBUTION STATEMENT (of the abstract entered in Block 20, if different from Report)		
18. SUPPLEMENTARY NOTES		
19. KEY WORDS (Continue on reverse side if necessary and identify by block number)  Fracture Mechanics                      Impact Crack Propagation                      Dynamic Photoelasticity Crack Arrest		
20. ABSTRACT (Continue on reverse side if necessary and identify by block number) A combined numerical and experimental procedure for evaluating some of the fracture dynamic parameters which govern the crack run-arrest response in a fracturing plate are discussed. A dynamic finite element code is used to compute the dynamic stress intensity factor and dynamic energy release rate, associated with a propagating crack which is driven by the experimentally determined crack velocity. Numerical results generated by the developed procedure are then compared with dynamic stress intensity factors obtained through dynamic photoelastic analyses of fracturing Homalite-100 plates. Two (OVER)		

DD FORM 1 JAN 73 1473

EDITION OF 1 NOV 65 IS OBSOLETE  
S/N 0102-014-6601

Unclassified

SECURITY CLASSIFICATION OF THIS PAGE (When Data Entered)

ABSTRACT (Continued)

edge-cracked specimens with fixed edge displacement loadings and two wedge-loaded double cantilever beam specimens were considered in this comparative study. Good agreements were obtained between the results obtained by the developed numerical-experimental procedure and dynamic photoelasticity.

DAT  
FILM